

Nonlinear behavior of the tarka flute's distinctive sounds

Arnaud Gérard,^{1,2} Luis Yapu-Quispe,³ Sachiko Sakuma,⁴ Flavio Ghezzi,¹ and Gonzalo Marcelo Ramírez-Ávila¹

¹*Instituto de Investigaciones Físicas, Universidad Mayor de San Andrés, Casilla 8635. La Paz, Bolivia*

²*Acústica StudioLab, Casilla 453, Potosí, Bolivia*

³*Instituto de Matemática e Estatística, Universidade Federal Fluminense. Niterói, Brazil*

⁴*Conservatorio Plurinacional de Música. La Paz, Bolivia*

The Andean tarka flute generates multiphonic sounds. Using spectral techniques, we verify two distinctive musical behaviors and the nonlinear nature of the tarka. Through nonlinear time series analysis we determine chaotic and hyperchaotic behavior. Experimentally, we observe that by increasing the blow pressure on different fingerings, peculiar changes from linear to non linear patterns are produced leading ultimately to quenching.

PACS numbers: 43.25.+y, 43.58.+z, 43.60.+d, 43.75.+a, 05.45.Tp, 05.45.Jn

Keywords: nonlinear acoustics; music and musical instruments; autocorrelation function; time series analysis; high-dimensional chaos

Our research provides a thorough nonlinear analysis of the acoustics of the tarka, a musical instrument played during Carnival in the Andean region of Bolivia, Southern Peru and Northwestern Argentina. While the musical properties of the tarka have been studied for many years, there is little analysis of its physical properties in particular an explanation for the instruments characteristic rasping timbre. The tarka produces two different musical sounds with different digitizations, the roll and non-roll. These sounds are multiphonic, generated by a monophonic instrument in which two or more pitches can be heard simultaneously. Time series analysis using concepts such as power spectra, autocorrelation function, chaoticity tests, phase space reconstruction, Lyapunov exponents, and entropy-complexity measures have been used to characterize the tarka's sounds. This interplay of spectral techniques, nonlinear analysis and the peculiarities of the tarka gives us a unique insight into the acoustics of artisanal instruments and furthermore an explanation relevant to other nonlinear generators.

I. INTRODUCTION

The tarka is a multiphonic musical wind instrument (Fig. 1) with an unusual timbre that is highly appreciated for its aesthetics amongst Andean communities¹⁻³. Multiphonic behavior has generated a great deal of interest among the scientific community.

Existing works and literature provide some relevant lines of study that could contribute to the explanation of the tarka's multiphonic behavior. The mainstreaming of multiphonic effects has been well documented⁴ and according to Maganza et al.⁵ many wind instruments belong to a class of nonlinear systems that exhibit very interesting behaviors, such as, the evolution from quasiperiodic to chaotic regimes. Fletcher⁶ studied the mode-locking favored by the nearly harmonic normal mode frequencies of a musical instrument and found that those instruments capable of maintaining a tone are essentially composed of one or more resonator systems that act in a markedly linear manner but are excited by a nonlinear source. Therefore the natural modes of a resonator are never really in perfect harmonic relations.

Having established the nonlinear nature of certain musical instruments and their respective sounds, Wilson and Keefe⁷ calculated Lyapunov exponents, correlation dimensions and the instability of tones in clarinets. While Keefe and Laden studied the correlation dimension of mul-

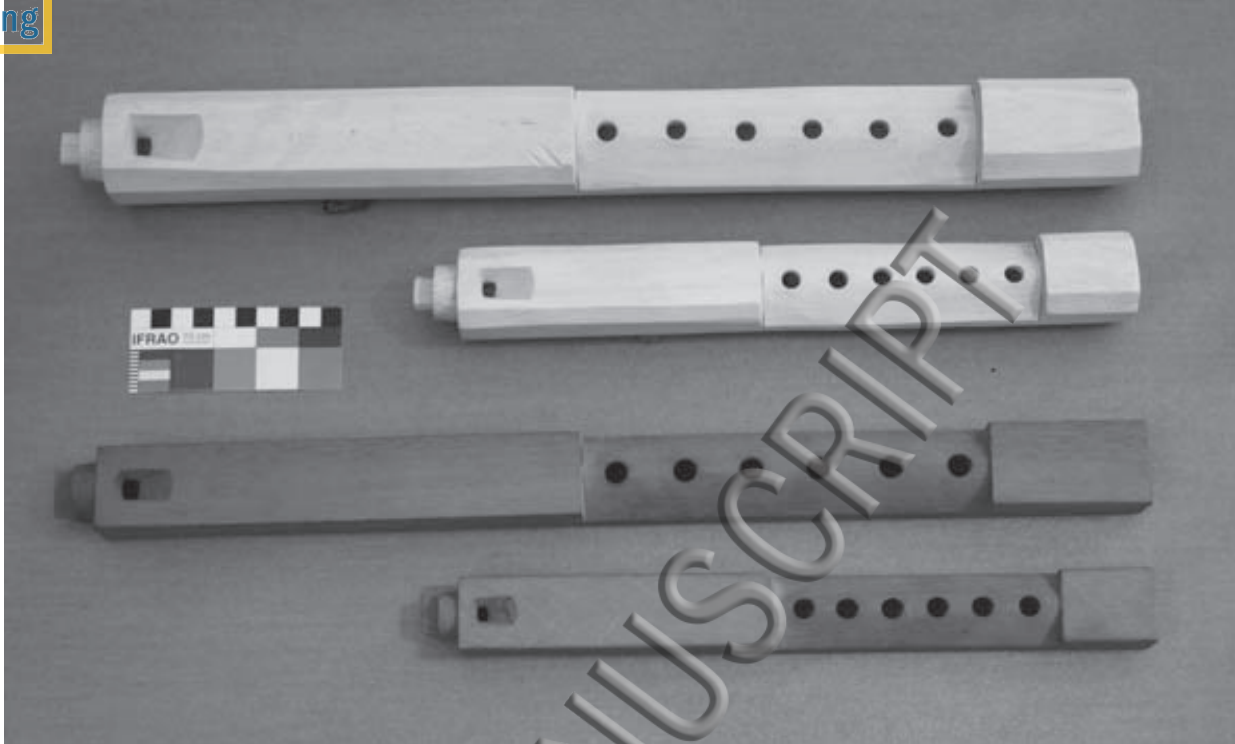


FIG. 1. Tarkas: the long and short instruments are known respectively as taikas (T) and malas (M). See also Section II for notation and sizes.

tiphonic tones of wind instruments⁴, in which they concluded that trajectories within the phase space of multiphonic sounds are examples of strange attractors and probably behave as chaotic systems. Furthermore, Lauterborn and Parlitz⁸ explained some of the implications of bifurcations and limit cycles in the context of acoustics.

Another approach was taken by Castellengo⁹, who related multiphonics to the presence of variations or discontinuities of the bore cross-section; the relative position, the diameter and the thickness of the finger holes.

The purpose of this work is to reveal the mechanisms behind the multiphonics of the tarkas distinct sound types. While these sounds can be differentiated acoustically there has been no physical understanding of this phenomenon^{1,2}. Using the above ideas we carried out spectral and nonlinear analyses with surprising and interesting results as will be explained within the paper. Our approach consisting in the interplay of spectral techniques, nonlinear analysis and the peculiarities of the tarka gives a unique insight into the acoustics of artisanal instruments and furthermore an explanation relevant to other nonlinear generators. In Section II, we give necessary notation and

definitions that are used within the paper. An explanation of the experimental details relevant to the spectral and nonlinear analysis are outlined in Section III. This analysis is used to determine and describe the specific features of the different sounds of the tarka. In Section IV we present final comments, conclusions and provide perspectives for further developments.

II. NOTATION AND DEFINITIONS OF TARKA

In order to have a uniform language and clear concepts on what concerns the characteristic sounds of the tarka, we detail notation used throughout the paper and give the definitions of roll and non-roll sounds.

A. Notation

Abbreviations are used to refer to the different notes or sounds. These are composed of a capital letter and a series of numbers. The letters T and M refer to the *taika* tarka, and *mala* tarka respectively. The numbers indicate the fingering, i.e., the finger holes covered (top to bottom) to produce a particular note. For example, T123 is a sound produced by a *taika* tarka in which the top three finger holes are covered. While T0 refers to a sound produced by the *taika* in which all the holes are uncovered.

We base our analysis on sounds produced by fingerings used by indigenous players of the tarka and also other fingerings relevant to the study, namely:

non-roll **T0, T1, T2, T3, T5, T25, T2345,**

M1, M123,

roll **T12, T123, T1234, T12345, T123456, T235, T23456, T3456,**

M12, M1234, M12345, M123456, M23456, M3456.

Those shown in boldface are the typical fingerings used by musicians.

B. Definitions of roll and non-roll sounds

When played at different blow pressures, the tarka has several distinguishable sounds described in Section IV B. However, the main focus of this study is a classification of the sounds aesthetically sought by experienced tarka musicians, played at an appropriate blow pressure with known

digitisations. These characteristic sounds are known as tara and non-tara^{1,2} and in this paper are referred to as the roll and non-roll.

A multiphonic roll sound is a hoarse, shrill and twangy sound^{9,10} showing a perceptible, periodic pulsation (modulation of amplitude) varying roughly between 1 Hz and 20 Hz. In order to produce the roll effect in a tarka the musician must blow energetically and accurately hook the right blow pressure which depends on the transient attack and the skill of the musician. The roll sound seems to have its origins in the inharmonicity of the partial tones. For our purposes we define the roll sound by means of the sonogram shown in Fig. 2. The roll sonogram shows a characteristic pattern with a very weak first fundamental and intense levels at 2 and 3 (octave and twelfth). The lines are interrupted periodically, i.e., they pulsate. This is also seen in the waveform where fluctuations in the envelope show a periodic increase and decrease in the amplitude or intensity. What is described in the sonogram and the waveform is a sound that is multiphonic with a roll effect⁹. For the non-roll sound (T1), Fig. 2 shows that the sonogram frequency lines are continuous and uniform. The most intense harmonics are 2, 1, 3, etc. in decreasing amplitude order; however, there is also a group of intense harmonics between 4 and 8 kHz which make the sound vociferous. We observe blow noise, characterized by the grey background in the sonogram.

III. EXPERIMENTAL METHOD AND SETUP

In this section, we first give the main features of a tarka from its construction point of view and also consider the cultural aspects related to the musicians playing the tarka. Thereafter, we describe the recording process and data collection protocols for the time series analysis.

The tarka is a type of duct flute which has a rather unusual rectangular shape (Fig. 1) and is usually made from wood such as mahogany (*Swietenia macrophylla-king*) or jacaranda (*Jacaranda mimosifolia*). It has a mouthpiece and six lateral finger holes but no thumbhole. The beak has a block with a windway which guides the air jet to the labium producing an edge tone effect. Tarkas have notable variations in their bore section, the internal shape is irregular resembling a bowed cylinder or stem vase, hereafter called vase shape (Fig. 3).

Tarkas are played together in a *tropa* (ensemble). This ensemble usually involves between 6 and 24 instruments of differing sizes; small, medium, and large in length. They are played together in parallel fourths, fifths and octaves, as well as, other intervals which are often dissonant producing

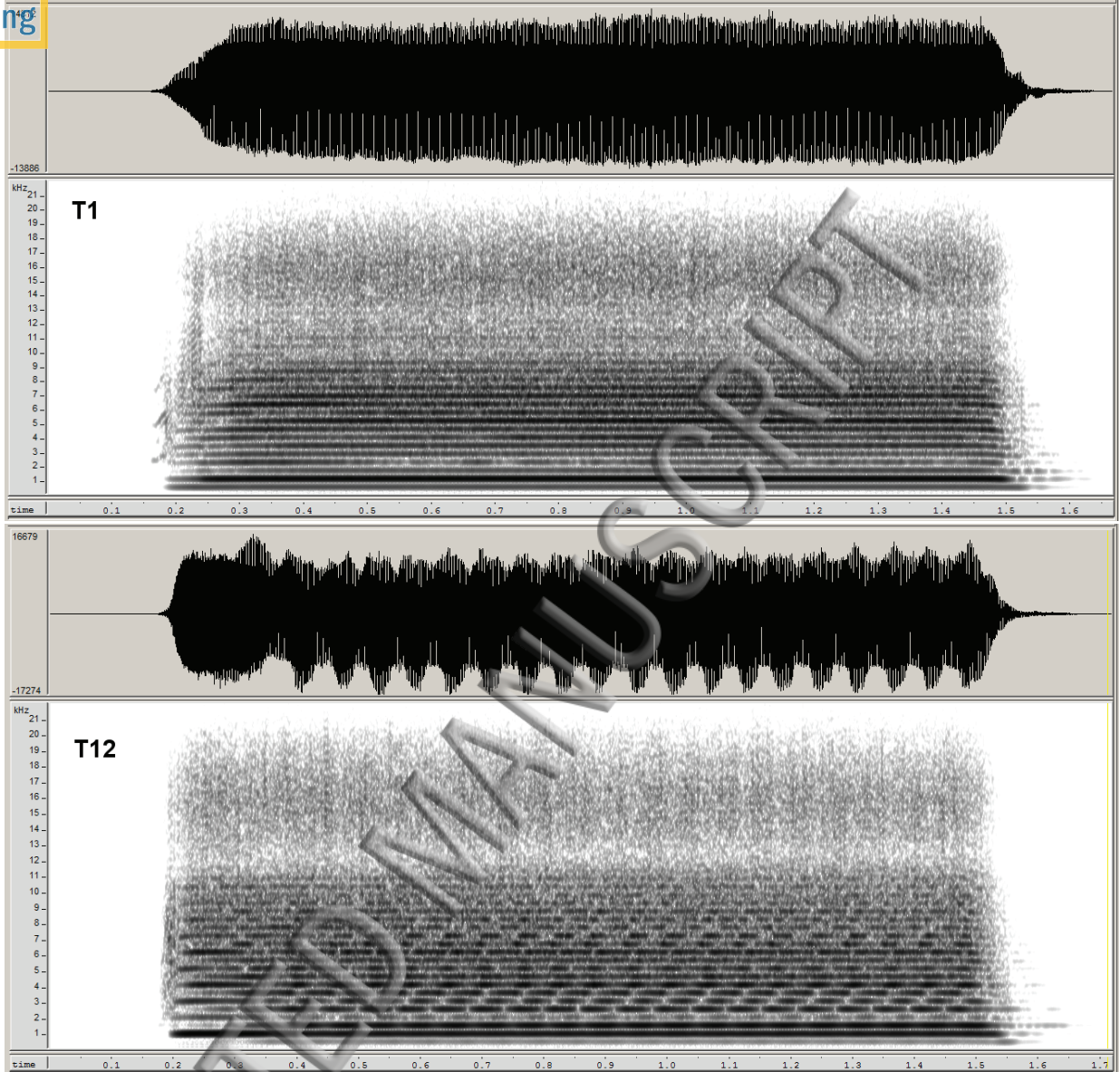


FIG. 2. Samples of waveforms and sonograms for the taika: the **non-roll** sound occurs when the first upper finger hole is covered (T1) and the **roll** sound when the first two upper finger holes are covered (T12). The sounds in the form of wav files are available as supplemental material¹¹.

the musical form known as *tarqueada*. Each region or community has its own acoustic preferences and ensembles, providing them with their own particular identity.

For this work, we mainly concentrate on the properties of two instruments of the tarka family, which exhibit typical acoustic behaviors¹. These tarkas were made in Hualata Grande (La Paz), the most prestigious village of ethnic flute makers in Bolivia.

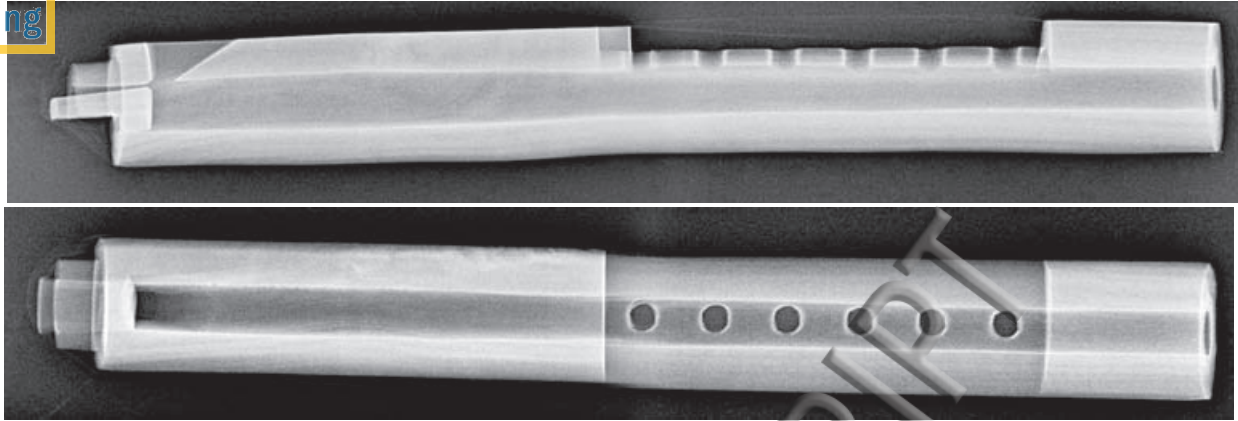


FIG. 3. X-ray images of a taika tarka in which we observe the typical vase-like shape of the internal hollow carved by the instrument maker with the aim of obtaining the instruments characteristic multiphonic sound. Note the difference in the geometry between the frontal and lateral views. The longitudinal length of the above taika is 41 cm. Image taken by Edwin Centeno, U.M.S.A.

The tarka flutes were measured: a medium sized (*taika*) and a small sized (*mala*) from a class of ensemble (*tropa*) called ullara. Table I and Fig. 4 show the tarka used, its characteristics and measurement studies including acoustic longitudes, hole diameter, and labium size. The mala is approximately one third shorter than the taika.

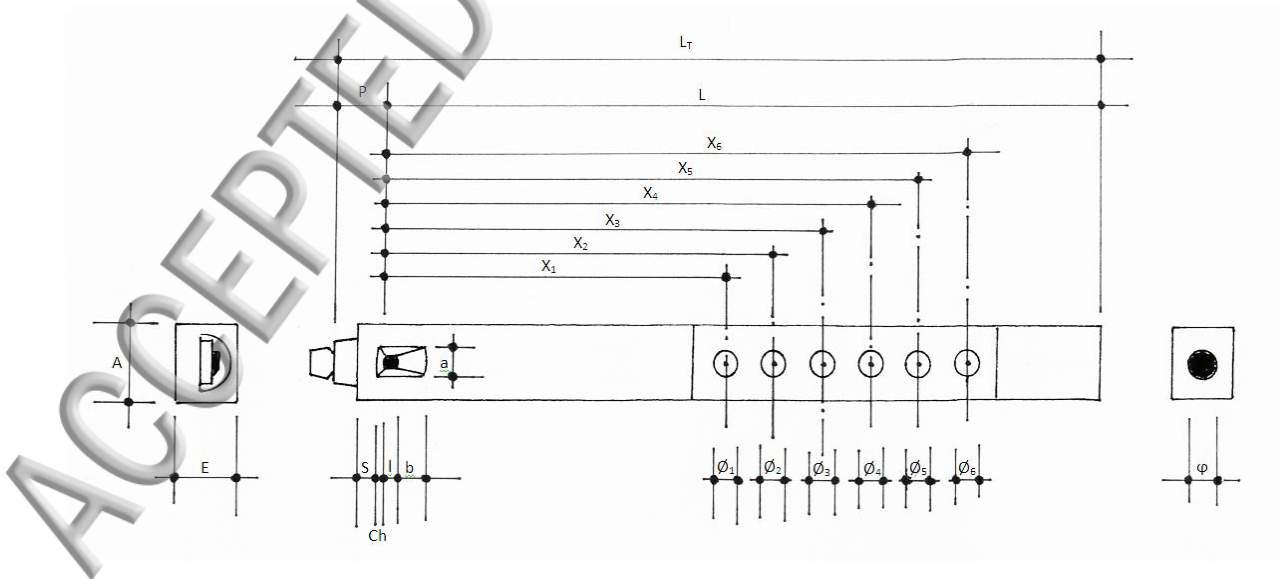


FIG. 4. Acoustic measures of the tarka. These measures are given in Table I.

Tarka	X_1	X_2	X_3	X_4	X_5	X_6	L
Taika	22.4	25.5	28.5	31.65	34.80	37.95	46.3
Mala	14.2	16.35	18.45	20.5	22.55	24.55	30.5

Tarka	P	I	S	a	b	Ch	A	E	φ	\emptyset_i
Taika	2.2	0.65	0.75	1.5	1.8	0.3	3.8	3.2	1.9	1.0
Mala	1.9	0.6	1.1	1.5	1.2	0.2	3.6	2.45	1.2	0.85

TABLE I. Measurements in centimeters of the taika and mala used to record the sounds and represented in Fig. 4. \emptyset_i is the bore diameter which is constant for all the finger holes ($i = 1$ to 6).

The sounds, played by A. Gérard, were recorded with a digital computer system in an anechoic chamber using Behringer ECM 8000 and dbx (flat frequency response) microphones and a recording software set to 16 bits and 44.1 kHz (sampling rate). For the analysis the data range was between 1 to $2^{16} = 65536$ points.

Guided by the sonograms we worked solely with the stable parts and eliminated the transient parts of attack and release. The same procedure was applied when we investigated the changes of regime due to variations in the blow pressure, i.e., we only considered the stable part of each regime. The duration of the time series were approximately 1.6 seconds for a constant blow pressure and around 4 seconds for increasing blow pressure.

IV. ANALYSIS

The first part of this Section looks at the spectral analysis of the recorded tarka sounds. We concentrate our analysis on the autocorrelation functions and power spectra while in the second part we look at nonlinear behavior using phase space reconstruction techniques¹²⁻¹⁴ and the computation of Lyapunov exponents and Kaplan-Yorke dimension of the attractors resulting from the reconstructed phase space. Our analysis is based on the use of TISEAN algorithms^{12,15} and whenever needed we checked our results with well known sounds such as the recorder or synthesis generated sounds and also by making our own programs.

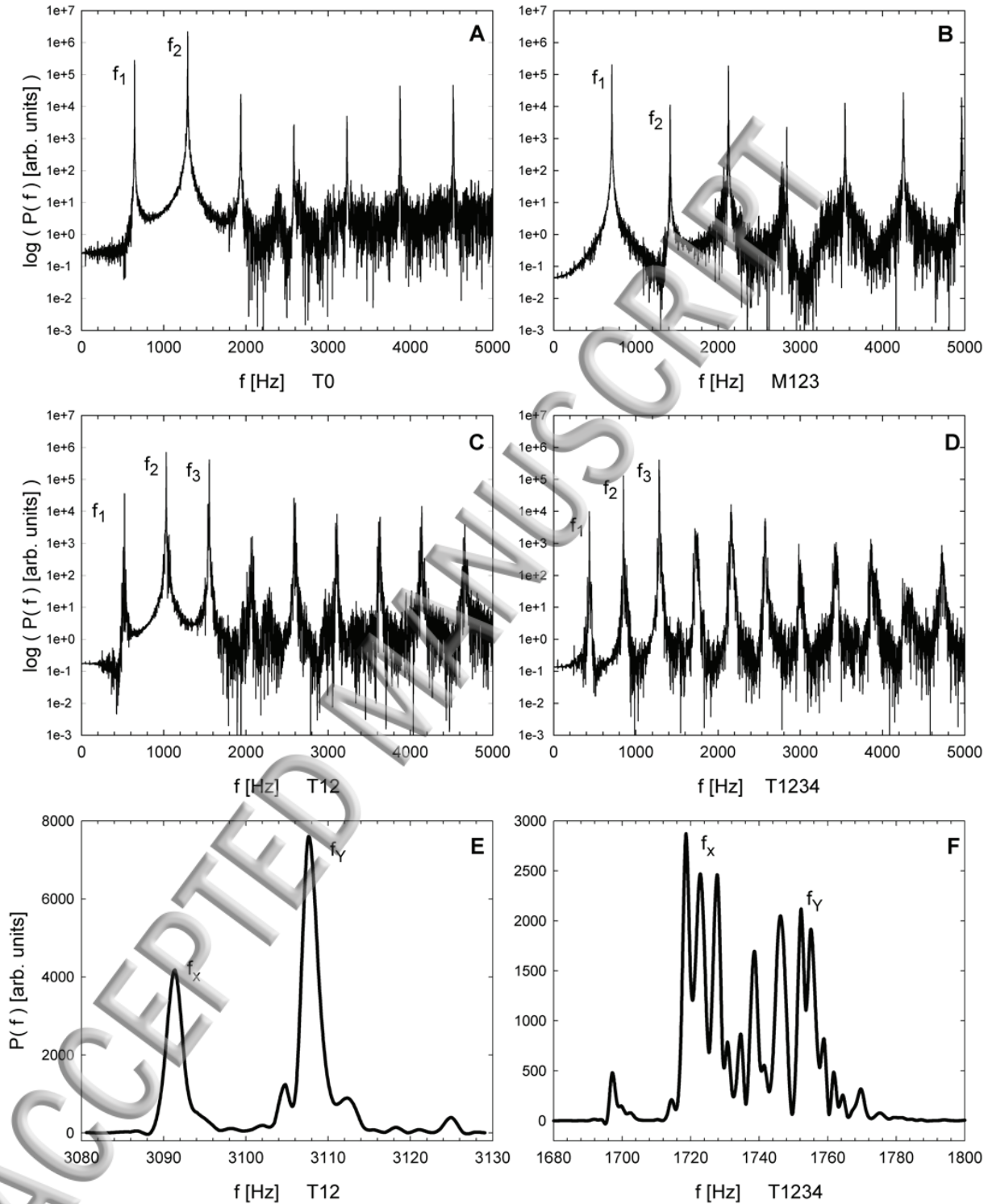


FIG. 5. Power spectra **A**, **B** of non-roll sounds with fingerings T0 and M123, **C**, **D** of roll sounds with fingerings T123 and T1234. Graphs **E**, **F** show peaks taken from specific frequency ranges of graphs C and D respectively. The distance between f_x and f_y contributes to the typical roll sound.

Spectral behavior

In the power spectra of the non-roll sound (Fig. 5) the intensity of the second frequency is generally higher than the first. The most notable exception is shown in Fig. 5B where the second frequency is much smaller in intensity than the first while the first and third frequencies have similar values in intensity. However, the ratio in all cases between the first two frequencies is equal to 2. Other lower intensity frequencies are integer multiples of the first frequency i.e., harmonic-like behavior.

	T12		T12345	
	f [Hz]	P(f) [arb. units]	f [Hz]	P(f) [arb. units]
f_1	490	5.75e-7	369	9.76e-8
	507	7.09e-6	388	2.43e-8
	523	3.61e-4	400	7.75e-5
	541	1.39e-6		
f_2	997	3.80e-6	770	7.94e-6
	1031	6.66e-3	786	1.04e-3
	1065	1.84e-5	800	4.56e-6
	1081	6.05e-6		
f_3	1503	8.05e-7	1171	2.53e-5
	1537	1.68e-4	1186	3.54e-3
	1554	3.88e-3	1217	1.75e-6
	1587	2.47e-6		
f_4	2011	8.67e-7	1554	1.05e-7
	2060	1.46e-5	1571	1.11e-6
	2078	1.59e-5	1585	1.36e-7
	2094	3.70e-6	1602	1.05e-7

TABLE II. The first frequencies of the power spectrum of the roll sounds with their respective intensities for T12 and T12345. The numbers in bold refer to the main peak. T12 is related to Fig. 5 C while T12345 is related to Fig. 8 A3.

The power spectrum frequencies for the roll sound are not harmonic and occur in bundles as

can be seen in Fig. 5 and Table II. The intensity of the second (f_2) or third (f_3) frequencies are the strongest and sometimes the intensity of the first frequency f_1 is very small. In Fig. 5 it can also be observed that for T12, f_2 is bigger than f_3 while for T1234, f_3 is more intense than f_2 . In addition, the frequencies are not multiples of the fundamental f_1 and obey the rules $f_3 = f_2 + f_1$ and $f_1 + f_4 = f_2 + f_3$. This behavior is observed in second harmonic generation systems¹⁶ and as $f_4 = f_1 + 2f_2$, we need a third order or cubic static nonlinearity to describe these components¹⁷. Furthermore, there are usually two peaks f_x and f_y separated by approximately 10 to 20 Hz one higher than the other. Sometimes the high peak is first and at other times it is second (Fig. 5). We found that this characteristic is present but not always clearly defined as in graph F of Fig. 5. An example of the contribution of these peaks to the composition of the roll sound is seen in the sonogram of T12 (Fig. 2) where it is clearly defined at higher frequencies. We observe a pattern similar to a brick and mortar wall of intercalated changes of frequency intensity. In addition, the different frequencies have these interruptions at different times. These pulsations seem to be responsible for the rasping beating effect heard in the roll sound.

Looking at the autocorrelation functions there exist two or more peaks of which one is always higher than the others, Fig. 6. Graphs A and B are for the non-roll sound with two different fingerings. Graph A shows a correlation pattern with a uniform amplitude showing two characteristic peaks. In graph B the uniformity of the amplitude continues; however, the pattern-form becomes more elaborated. Graphs C and D are for the roll sound and we observe through the correlation functions a more complicated behavior of the peaks which will be further discussed in Section IV C and seems to be related to its hyperchaotic behavior. In all cases with similar patterns to those seen in graphs C and D we find two positive Lyapunov. Whereas in the cases exemplified in graphs E and F for the roll sound there is only one positive Lyapunov exponent and consequently no hyperchaos is present.

The observed peaks in the autocorrelation function for the roll sounds in Fig. 6 are related to the second harmonic resonance found, i.e., $f_1 + f_4 = f_2 + f_3$.

B. Analysis of increasing blow pressure

When a musician increases the blow pressure in a linear manner the jumps between regimes in the sonogram are notable. By increasing the blow pressure of the excitation system, the tube successively changes regimes permitted by the geometry of the resonator from mode 1 (fundamental)

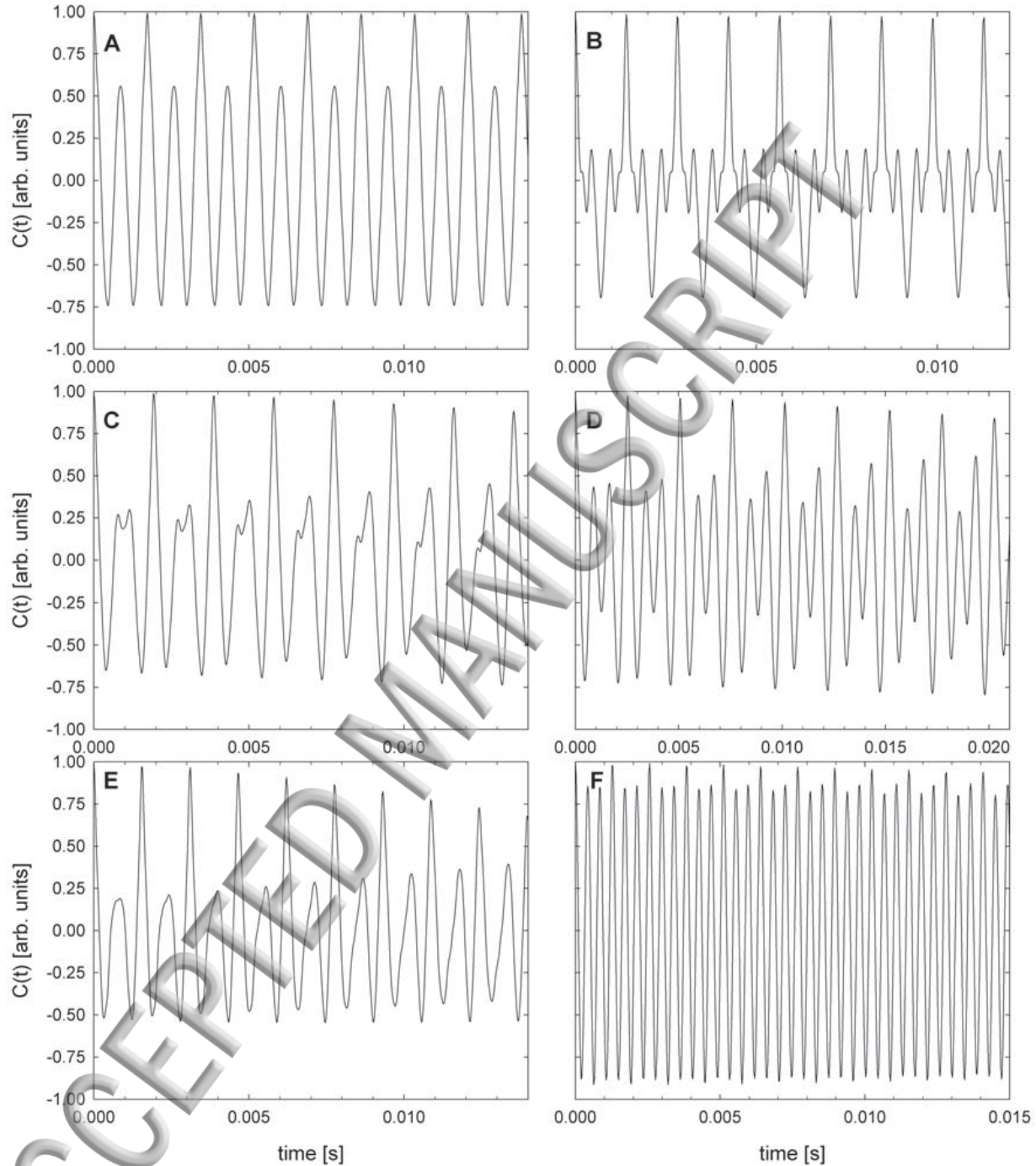


FIG. 6. **A**, **B** show the variety of autocorrelation functions observed for non-roll (**A** is T1 and **B** is M123). **C**, **D** show typical functions for roll sounds that are associated with hyperchaos (**C** is T12 and **D** is T12345). Finally, **E**, **F** refer to roll sounds associated with chaos but not hyperchaos; in **E**, the two small peaks observed in **C** are not well defined while in **F** these peaks change very slowly with time (**E** is M12 and **F** is M1234).

to mode 2 (harmonic 2) and then mode 3 and so on (successively). In each of the modes a regime is established, that is a special harmonic configuration, with partials and noise that form a certain sound structure that is particular to each case¹⁸. However, in the case of the tarka (Fig. 7), something unusual occurs. In this paper, we describe the variety of spectral and nonlinear phenomena observed leaving the acoustical analysis such as acoustic regimes for further work (Figs. 8 and 9).

Another observed phenomenon is quenching (Fig. 10) which occurs in self-sustained oscillators when the amplitude increases due to high blow pressures and thereafter suddenly plummets. It is a well-known phenomenon in coupled systems and is generally due to high values of the coupling strength which acts on the interaction of the excitatory source with the resonator¹⁹⁻²¹. This phenomenon occurring in coupled oscillators is related to the emergence of amplitude and oscillation death²² that may be manifested totally or partially¹⁹, and is produced by means of time-delay or by strong coupling²³. The mechanisms of oscillation quenching are explained widely²⁴, and different transitions from amplitude to oscillation death²⁵.

In order to exemplify the observed phenomena, we look at the roll and non-roll cases shown in Fig. 7. For the type of analysis used in this paper we only focus on the stable parts which in both cases are four.

For the roll case, each stable part (A1, A2 and A4) exhibits its highest intensity peak first and then follows with lower peaks which are multiples of the highest intensity peak as shown in Fig. 8. Whereas the third stable part (A3) has its third frequency higher than the second which in turn is higher than the first. This behavior has already been described when T12345 was observed as a whole sound¹¹.

For the non-roll sound T1 in Fig. 8, in all the stable parts B1 to B4, the frequencies are multiple integers of the fundamental. However, in this case the changes in intensity are responsible for the different phenomena. In B1, the fundamental has the highest intensity, in B2 the intensities of the fundamental and the second harmonic are similar while in B3 the second harmonic is much higher than the fundamental. Finally in B4 the second harmonic becomes the fundamental with its respective harmonics; this jump is well known and has been explained above with the respective literature¹⁸. Looking at the changes with time, we see that the autocorrelation function is a well behaved single distribution for B1 and B4, in B3 we see the typical behavior for the non-roll. An interesting feature occurs in B2 where we observe the onset of the non-roll phenomenon. For completeness and comparison we include in Fig. 9 the autocorrelation functions for the roll case where we see more abruptly changes in the different patterns.

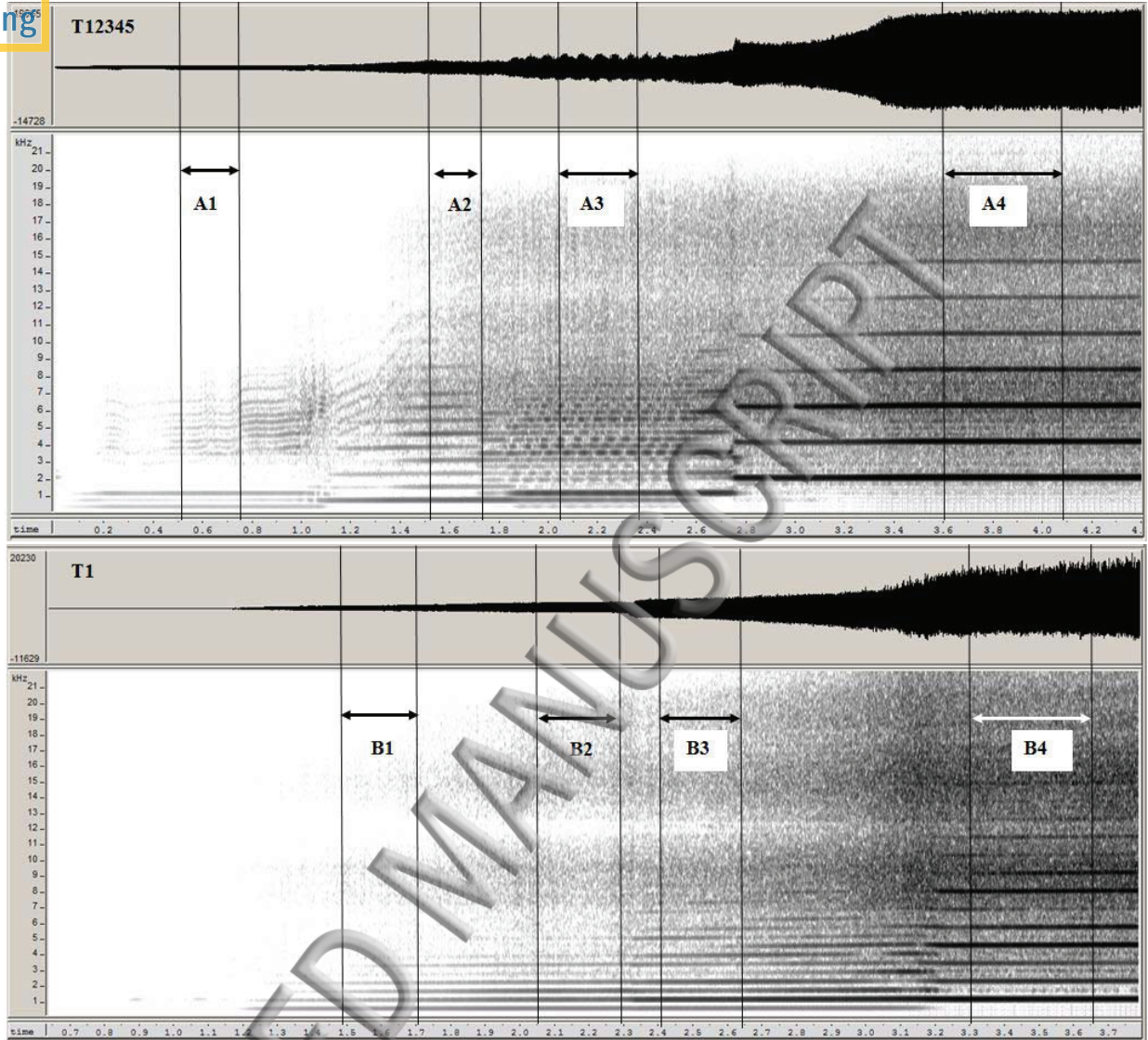


FIG. 7. Waveforms and sonograms obtained by gradually increasing the blow pressure for the roll sound (T12345) above and for the non-roll sound (T1) below. Sections are marked and correspond to stable parts which were analysed. Note that the blow pressure for A1 (p_{A1}) is less than the other parts, i.e., $p_{A1} < p_{A2} < p_{A3} < p_{A4}$. The same applies to the T1 sound and B parts, i.e., $p_{B1} < p_{B2} < p_{B3} < p_{B4}$. The sounds in the form of wav files are available as supplemental material¹¹.

C. Analysis of the nonlinear dynamics of *taikas* and *malas*

Given the nonlinear tendencies observed in the regions A3 and B3 and to further understand the dynamics we use standard nonlinear techniques to analyze the system. With this aim we carried out periodicity tests which do not show any periodic behavior in the considered digitizations. We

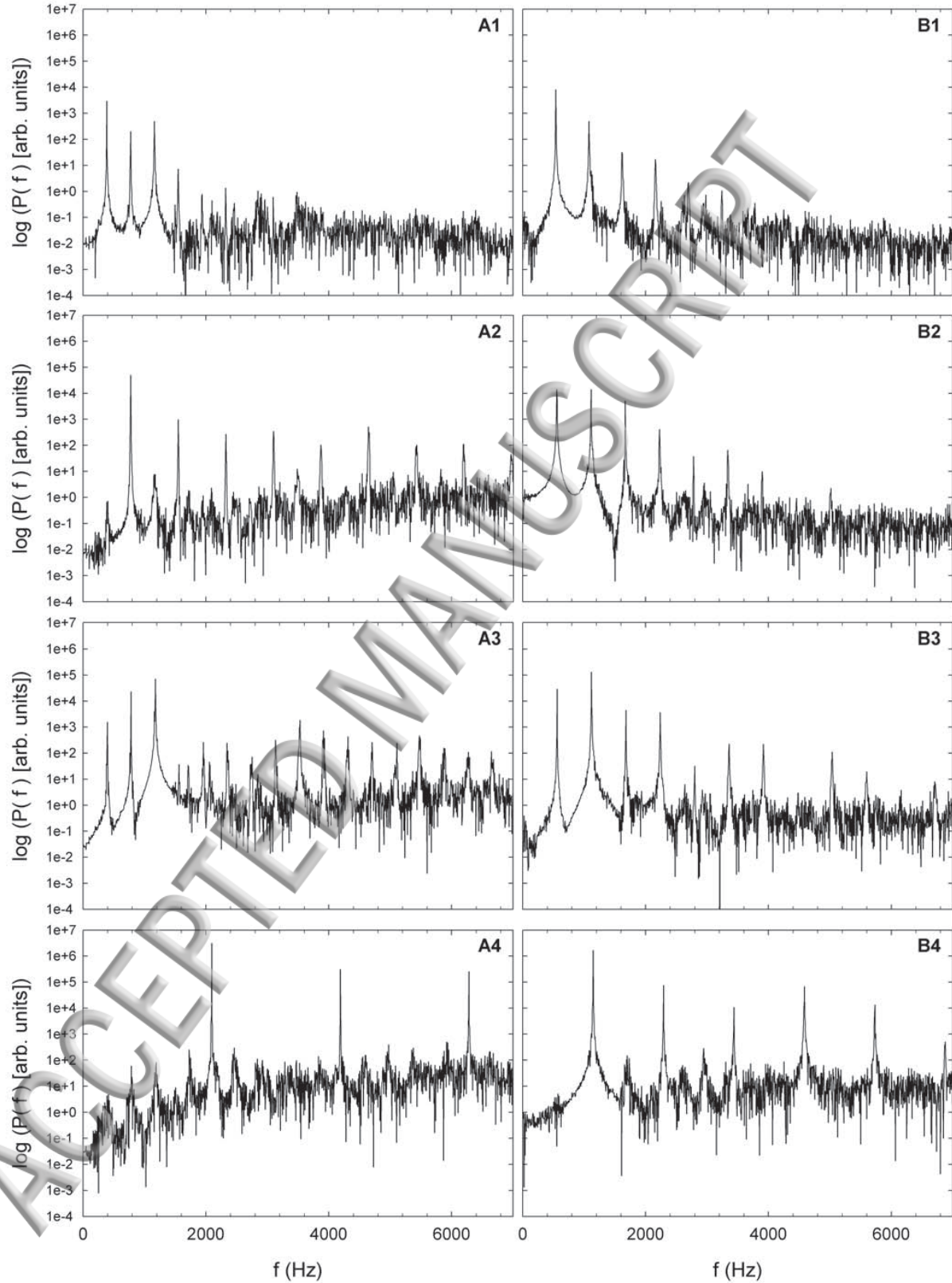


FIG. 8. Power spectra of the different stable parts when the blow pressure is varied: **A1, A2, A3, A4** are for T12345 and **B1, B2, B3, B4** are for T1. These graphs are related to the sonograms in Fig. 7.

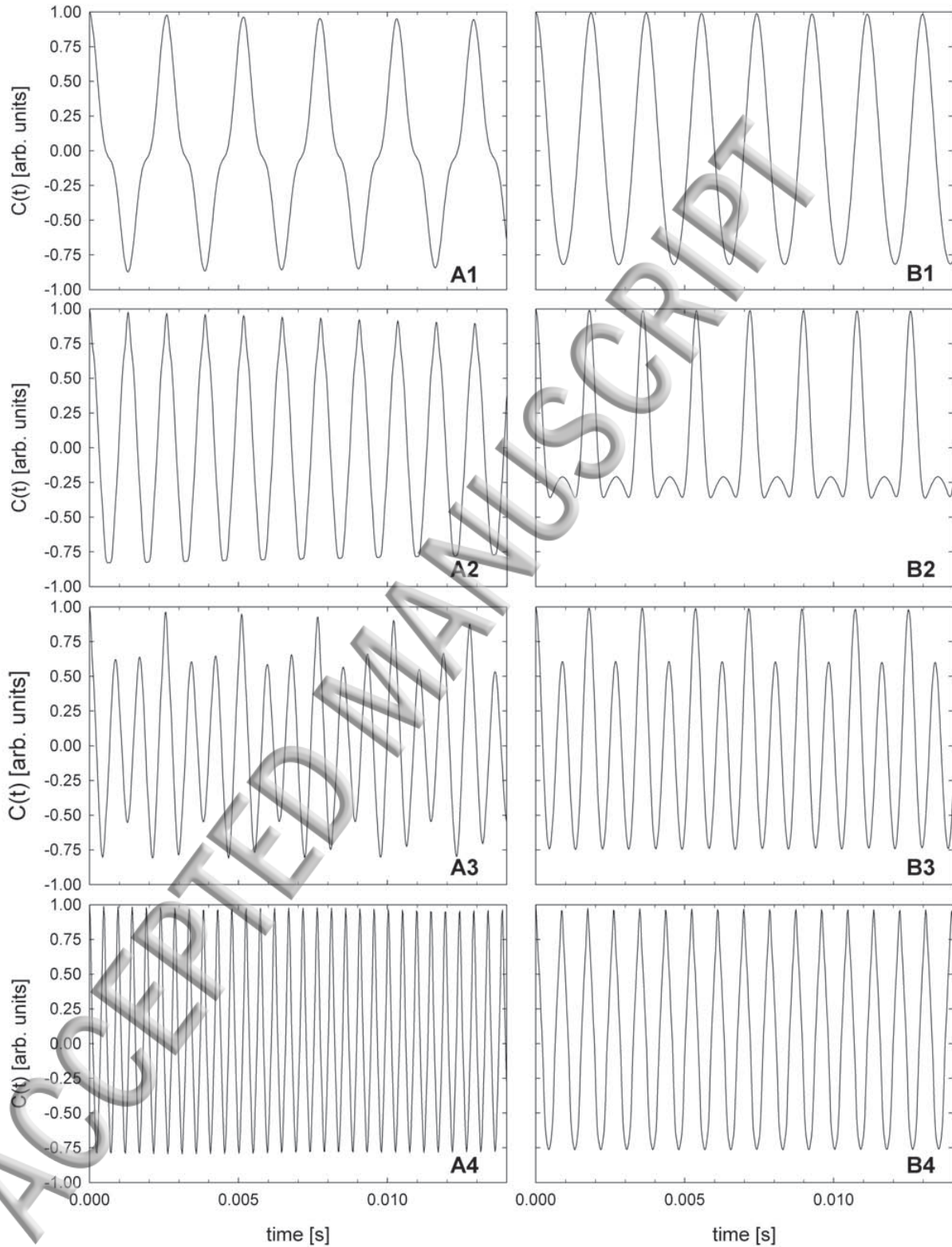


FIG. 9. Autocorrelation functions of the different stable parts when the blow pressure is varied: **A1**, **A2**, **A3**, **A4** are for T12345 and **B1**, **B2**, **B3**, **B4** are for T1. See the corresponding power spectra and phase spaces for a more complete picture of the increased blow pressure.

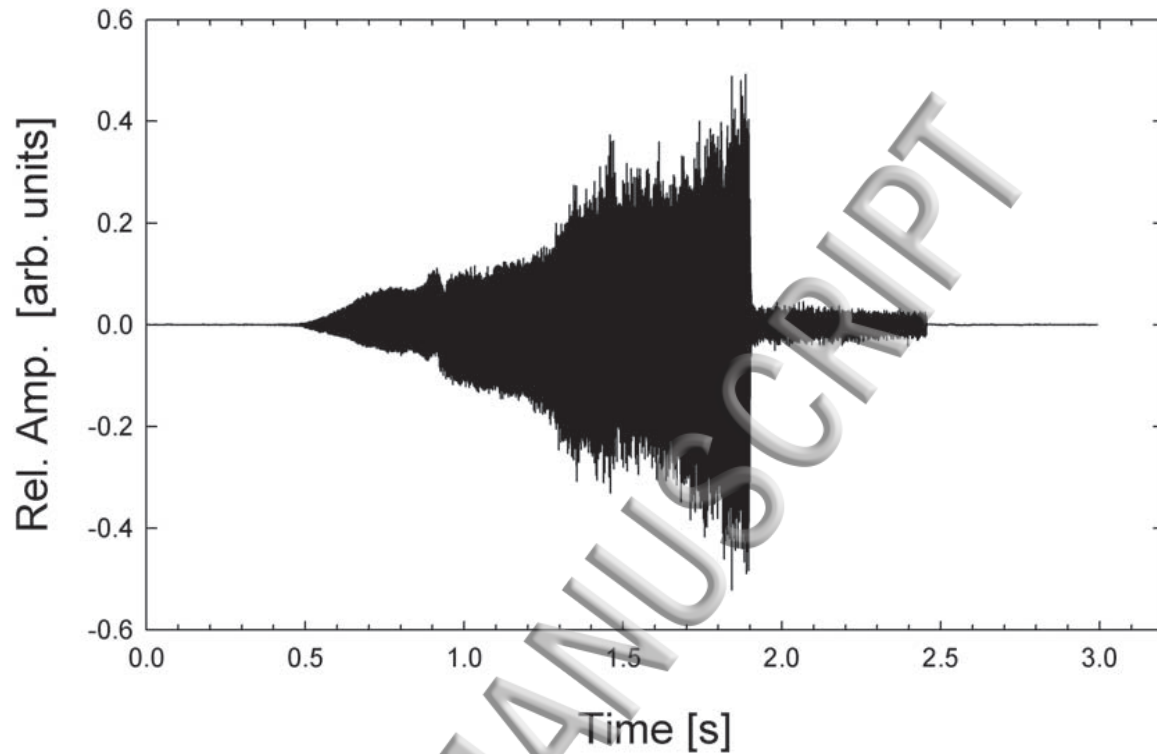


FIG. 10. The evolution of the observed waveforms of T1 when one increases the pressure. We clearly see the phenomenon of quenching as a result of the coupling.

also performed ϵ_1 tests²⁶ in order to determine whether the time series are chaotic or not. Then the phase space was reconstructed using the time lag and the embedding dimension. This was followed by the computation of Lyapunov exponents and the Kaplan-Yorke dimension which determine whether the system's behavior is chaotic or hyperchaotic²⁷⁻³⁰. Additionally, other techniques were explored, such as, the resampling of time series to improve the statistics for the determination of the Lyapunov exponents^{31,32}. Also, recurrence plots³³ and their implications on distinguishing hyperchaotic-chaotic transitions³⁴ were investigated, as well as, the construction of complexity vs. entropy planes^{35,36}.

In order to obtain the embedding dimension and therefore reconstruct the phase space from the time series, firstly, we compute the time lags by means of the autocorrelation function or the mutual information. Then, with the obtained time lags, the embedding dimension is computed by the method of false nearest neighbors. Once the above mentioned quantities are obtained, the

Lyapunov exponents and Kaplan-Yorke dimension were also computed from the time series by means of the Sano and Sawada algorithm³⁷. The most relevant results of the main fingerings are shown in Table III.

As mentioned above, we reconstructed the phase space using the time series corresponding to the parts A3 and B3 (see sonograms of Fig. 7). These parts are related to the musical sonority of the Tarka which is our particular interest. The non-roll sounds have one positive Lyapunov

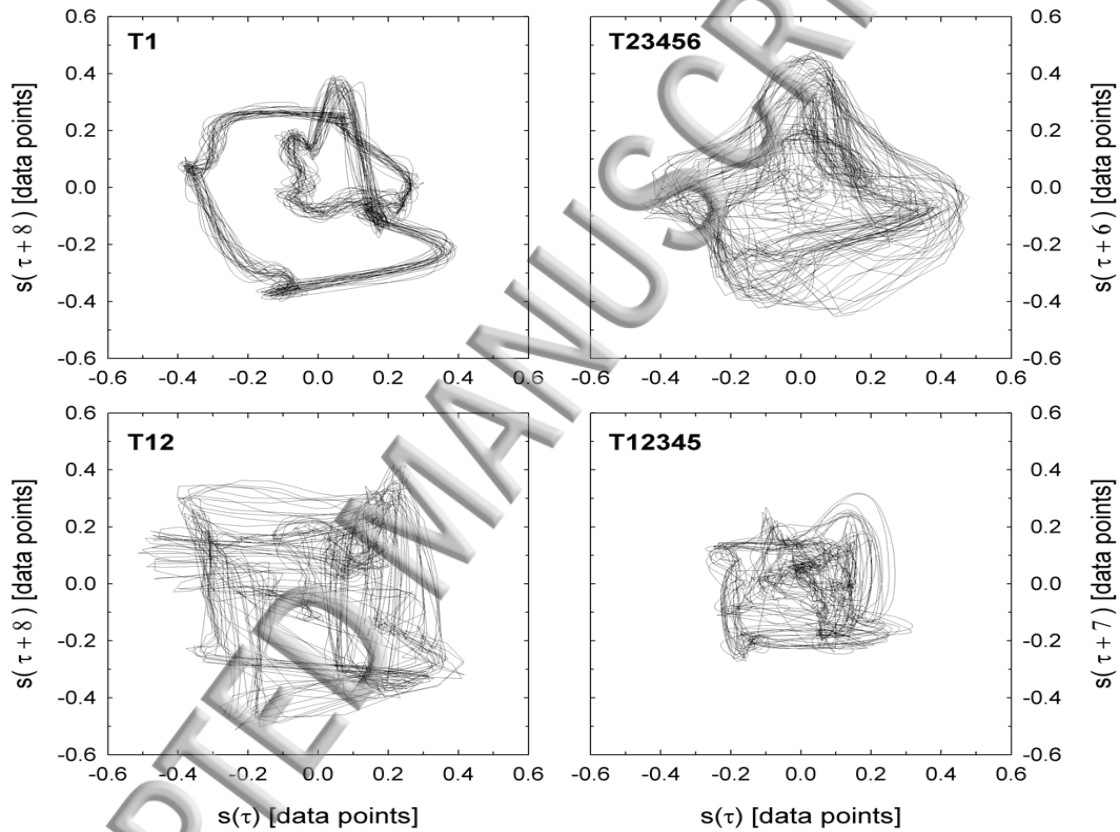


FIG. 11. Projection of the attractors corresponding to the time series of different digitizations. T1 is for a non-roll case, T23456 is for a chaotic roll sound. T12 and T12345 are examples of hyperchaotic attractors. The four images are for 3000 data points. Note that the numbers seen in the y-axis refer to the time lags as explained in the text.

exponent in part B3 of the sonogram shown in Fig. 7, thus, exhibiting chaotic behavior. For the roll sounds, in the taika most of the digitizations have two positive Lyapunov exponents which indicates hyperchaotic behavior; T235 and T23456 being the exceptions where the behavior is chaotic. In the case of the mala, only M12345 has two positive Lyapunov exponents.

Fingering	sound	time lag	embedding dim.	Lyapunov exponents			D_{KY}	$z1$
T0	non-roll	8	8	0.0266 ± 0.0011	-0.0174 ± 0.0008	-0.0531 ± 0.0008	2.1737 ± 0.0107	0.9922 ± 0.0016
T1	non-roll	11	8	0.0195 ± 0.0009	-0.0276 ± 0.0008	-0.0606 ± 0.0012	1.7089 ± 0.0432	0.8914 ± 0.0185
T25	non-roll	11	9	0.0368 ± 0.0007	-0.0051 ± 0.0014	-0.0329 ± 0.0011	2.9649 ± 0.0228	0.9859 ± 0.0039
M1	non-roll	7	7	0.0095 ± 0.0006	-0.0443 ± 0.0009	-0.0868 ± 0.0011	1.2145 ± 0.0111	0.8743 ± 0.0194
M123	non-roll	9	7	0.0190 ± 0.0007	-0.0388 ± 0.0008	-0.0844 ± 0.0014	1.4908 ± 0.0189	0.9799 ± 0.0045
T235	roll	5	5	0.0532 ± 0.0004	-0.0682 ± 0.0006	-0.1863 ± 0.0006	1.7803 ± 0.0059	0.9655 ± 0.0066
T23456	roll	5	6	0.1579 ± 0.0003	-0.0151 ± 0.0001	-0.1957 ± 0.0004	2.7297 ± 0.0010	0.9522 ± 0.0098
M12	roll	5	5	0.0756 ± 0.0005	-0.0559 ± 0.0007	-0.2064 ± 0.0009	2.0952 ± 0.0034	0.8764 ± 0.0166
M1234	roll	5	5	0.0949 ± 0.0007	-0.0256 ± 0.0006	-0.1415 ± 0.0007	2.4902 ± 0.0020	0.8368 ± 0.0206
T12	roll	11	8	0.0769 ± 0.0006	0.0122 ± 0.0004	-0.0374 ± 0.0010	3.6442 ± 0.0108	0.9161 ± 0.0150
T123	roll	10	6	0.1192 ± 0.0006	0.0044 ± 0.0004	-0.0835 ± 0.0009	3.2390 ± 0.0019	0.8830 ± 0.0180
T1234	roll	9	6	0.1243 ± 0.0005	0.0095 ± 0.0007	-0.0864 ± 0.0004	3.2627 ± 0.0021	0.9136 ± 0.0156
T12345	roll	11	7	0.0913 ± 0.0006	0.0052 ± 0.0009	-0.0614 ± 0.0006	3.2939 ± 0.0066	0.9807 ± 0.0048
T123456	roll	8	6	0.1066 ± 0.0002	0.0046 ± 0.0001	-0.0852 ± 0.0006	3.1480 ± 0.0021	0.9206 ± 0.0138
T3456	roll	7	6	0.1229 ± 0.0003	0.0192 ± 0.0003	-0.0716 ± 0.0002	3.4432 ± 0.0014	0.9109 ± 0.0161
M12345	roll	9	6	0.0522 ± 0.0006	0.0021 ± 0.0007	-0.0360 ± 0.0006	3.2661 ± 0.0091	0.9867 ± 0.0034

TABLE III. Time lag, embedding dimension, three largest Lyapunov exponents, Kaplan-Yorke dimension D_{KY} and factor $z1$ for the three observed cases: non-roll, roll chaotic and roll hyperchaotic. The table shows the values corresponding to the main digitizations that are representative of the three cases.

The estimation of the Kaplan-Yorke dimensions D_{KY} (Table III) shows that for hyperchaotic digitizations the Kaplan-Yorke dimension is greater than three.

In graph T1 of Fig. 11, a typical non-roll sound is shown. All the non-roll sounds of the tarka show this loop geometry, suggesting the existence of a homoclinic orbit. There are two cases to consider for the roll sound and these are shown in Fig. 11: a chaotic example seen in graph T23456 and two hyperchaotic examples in graphs T12 and T12345. These projections show similarities with well-known chaotic and hyperchaotic attractors found in the literature (see for instance³⁸⁻⁴¹ among others).

Taking into account the resampling method, we generated new time series for some digitizations, namely T0, T12, M1 and M12345, and computed the Lyapunov spectra for these new resampled time series obtaining similar results to those of the original series. These results reinforce, a priori, our assertions concerning the chaotic (found for non-roll sounds) and hyperchaotic (mainly found in roll sounds) behavior.

As stated above, the $z1$ factor measures the chaotic features of the time series. When the $z1$ value is close to zero the time series is regular and when it is close to one it is chaotic²⁶. Fig. 12(a) shows the evolutions of the $z1$ factor for typical digitizations for non-roll (T0 and M1) and roll (T12 and M12345) sounds. We note that for the non-roll sounds, the evolution towards a value of one is quicker than for the case of roll sounds this is also manifested in Table III. In general, the $z1$ uncertainties associated with roll sounds are greater than those corresponding to non-roll sounds. Recently, new interesting techniques for measuring complexity have been proposed^{35,36} and we have used these to obtain preliminary results of complexity and entropy measures for the studied time series as shown in Fig. 12(b). It is interesting to note that different sounds tend to occupy certain well-defined regions of the plane complexity vs. entropy and this could be useful for the classification of sounds and even instruments.

V. CONCLUSIONS AND PERSPECTIVES

The tarka has a single excitatory source and is designed in such a way that certain fingerings with the appropriate applied air jet pressure produce two physically distinct acoustic behaviors: the roll and non-roll sounds.

From diverse analyses, we claim the existence of chaotic and hyperchaotic behavior associated with non-roll and roll sounds respectively. Looking in more detail at the two distinctive types

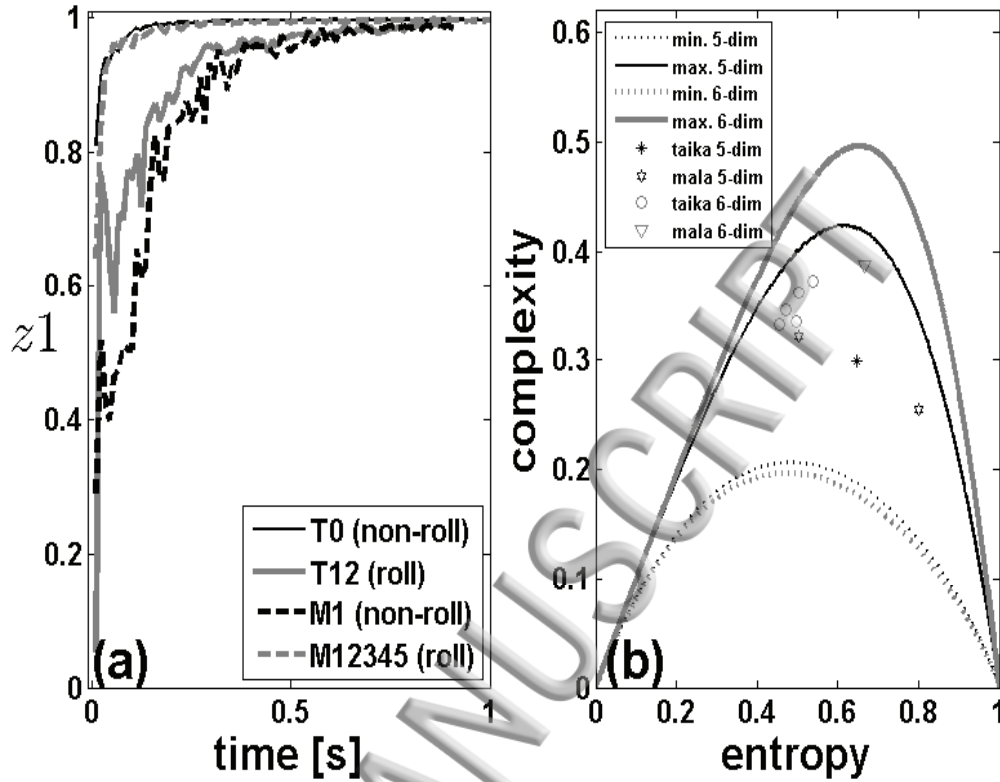


FIG. 12. (a) Evolution of the z_1 factor that measures the chaotic features for the time series corresponding to the digitizations T0, T12, M1 and M12345. (b) Plane complexity vs. entropy for embedding dimensions 5 and 6 whose minimum and maximum borderlines are clearly defined. The measures of complexity and entropy for the digitization time series with embedding dimensions (5 and 6) are also shown on the plane.

of sound we observe that the non-roll sound exhibits in its power spectrum a second harmonic higher than the first and according with our results has one positive Lyapunov exponent. While the second harmonic-like generation behavior of the roll sound suggests that any future model should be based on an anharmonic oscillator equation⁴².

The asserted chaotic and hyperchaotic behaviors of the roll sound seem to be associated with the interplay of the different peaks observed in the autocorrelation function. This can also be seen in the power spectra where the relationship between the first three frequencies is very important. In the case of the taika, the first three intensities are well defined while the mala has less defined intensities. It does not seem to matter whether the intensity of the second frequency is higher than the third, or the other way round. Currently we are not in a position to model the hyperchaotic

behavior observed. The distinctive beating heard in the roll sound might best be modeled on the ideas of Sliwa et al.⁴³.

The roll and non-roll sounds are observed in different fingerings and both are bounded by two linear parts (A1 and A4 or B1 and B4 respectively) when the blow pressure is changed. If the blow pressure is very high quenching occurs.

The geometrical aspects of the tarka suggest that chaos and hyperchaos are related to the nonlinearities observed in this instrument, and coincide with the sound (musical sonority) sought by the instrument maker and musician. Moreover, these intrinsic nonlinearities might enhance the nonlinear perception of the hearing system as stated by Cartwright et al⁴⁴.

We are aware that the nonlinear measures of chaoticity and complexity require special attention and careful analysis in order to reinforce our results. To this end we have considered new techniques and the suggestions for nonlinear time series analysis made in⁴⁵ to obtain a deeper insight into the complex sounds produced by this wind instrument.

In this paper we have presented the phenomenological behavior of the tarka further unraveling the mystery behind the tarka's rare and unusual timbre. The time series analysis applied to the tarka sounds allowed us to improve the understanding of the acoustical aspects of this instrument. This and future studies such as a thorough aerodynamical and geometrical analysis and controlled pressure experiments can help towards a more complete understanding of the link between acoustics, artisanal instrument fabrication techniques and the musical aesthetic of Andean communities.

ACKNOWLEDGMENTS

We would like to acknowledge G. Mindlin of Universidad de Buenos Aires for fruitful discussions and his interest in the tarka. Our thanks also go to E. Centeno for his helpful work taking the radiographic images of a taika. Also, we acknowledge S. Depickère for her helpful comments on the statistical aspects and to K. Byrne for the careful reading of the manuscript. Finally, thanks to the referees for their thoughtful input that improved this work.

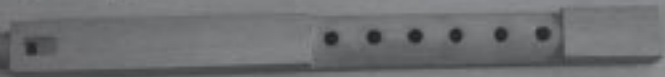
REFERENCES

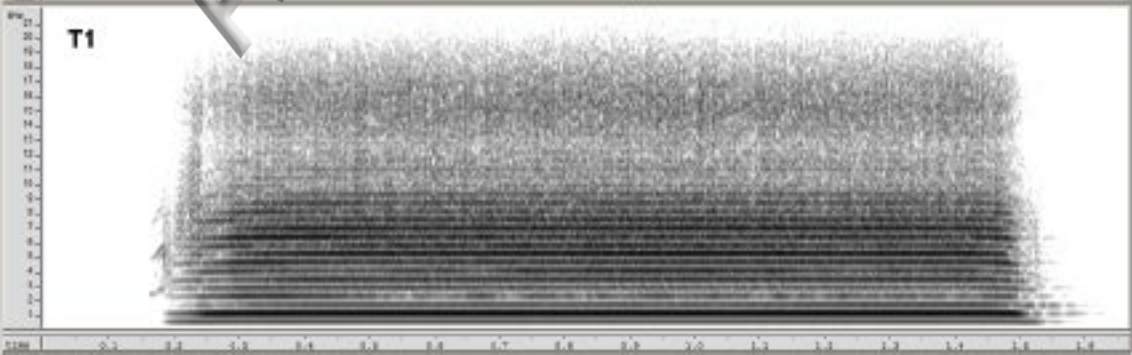
REFERENCES

- ¹A. Gérard, “Tara y tarka. Un sonido, un instrumento y dos causas (Estudio organológico y acústico de la tarka),” en *Diablos tentadores y pinkillus embriagadores en la fiesta de Anata/Phujllay. Estudios de antropología musical del carnaval en los Andes de Bolivia*, Vol 1, edited by A. Gérard (Plural editores, La Paz, 2010), pp. 69–140.
- ²H. Stobart, “Tara and Q’iwa - Worlds of Sounds and Meaning,” in *Cosmología y Música en los Andes*, edited by Max Peter Baumann (International Institute for Traditional Music, Vervuert Iberoamericana, Berlin, 1996), pp. 67–81.
- ³H. Stobart, *Music and the Poetics of Production in the Bolivian Andes*, (SOAS Musicology Series-Ashgate, United Kingdom 2006).
- ⁴D. Keefe, and B. Laden, “Correlation dimension of Woodwind multiphonic tones,” *J. Acoust. Soc. Am.* **90**, 1754–1795 (1991).
- ⁵C. Maganza, R. Caussé, and F. Laloë, “Bifurcation, period doubling and chaos in clarinet like systems,” *Europhys. Lett.* **1**, 295–302 (1986).
- ⁶N. H. Fletcher, “Mode locking in nonlinearly excited inharmonic musical oscillators,” *J. Acoust. Soc. Am.* **64** 1566–1569 (1978).
- ⁷T. D. Wilson, and D. H. Keefe, “Characterizing the Clarinet Tone: Measurements of Lyapunov Exponents, Correlation, Dimension and Unsteadiness,” *J. Acoust. Soc. Am.* **104**, 550–561 (1998).
- ⁸W. Lauterborn, and U. Parlitz, “Methods of chaos physics and their application to acoustics,” *J. Acoust. Soc. Am.* **84**, 1975–1993 (1988).
- ⁹M. Castellengo, *Sons Multiphoniques aux Instruments a Vent*, (Rapports IRCAM Nr. 34/82, Paris, 1982).
- ¹⁰E. Leipp, *Acoustique et Musique*, (Masson, Paris, 1976).
- ¹¹See supplemental material at URL... for the sounds corresponding to the waveforms and sonograms of the digitizations: T1 (T1.wav file for the non-roll sound), T12 (T12.wav file for the roll sound), T12345 (T12345.wav another example of roll sound); T1(hp).wav and T12345(hp).wav for the sounds with increasing blow pressure (hp). The sound files were provided by A. Gérard, Acústica StudioLab.

- ¹²H. Kantz, and T. Schreiber, *Nonlinear Time Series Analysis*, (Cambridge University Press, Cambridge, 2003).
- ¹³F. Takens, “Detecting strange attractors in fluid turbulence,” in *Dynamical Systems and Turbulence*, edited by D. Rand, and L. S. Young, (Springer, Berlin, 1981), pp. 366–381.
- ¹⁴T. Sauer, J. A. Yorke, and M. Casdagli, “Embedology,” *J. Stat. Phys.* **65**, 579–616 (1991).
- ¹⁵R. Hegger, H. Kantz, and T. Schreiber, “Practical implementation of nonlinear time series methods: The TISEAN package”, *Chaos* **9**, 413–435 (1999).
- ¹⁶J. A. Armstrong, N. Bloembergen, J. Ducuing, and P. S. Pershan, “Interactions between Light Waves in a Nonlinear Dielectric,” *Phys. Rev.* **127**, 1918–1939 (1962).
- ¹⁷A. H. Nayfeh, and D. T. Mook, *Nonlinear Oscillations*, (John Wiley & Sons Inc., New York, 1995).
- ¹⁸N. H. Fletcher, “Acoustical correlates of flute performance technique,” *J. Acoust. Soc. Am.* **57**, 233–237 (1975).
- ¹⁹F. M. Atay, “Total and partial amplitude death in networks of diffusively coupled oscillators,” *Physica D* **183**, 1–18 (2003).
- ²⁰D. V. Ramana Reddy, A. Sen, and G. L. Johnston, “Experimental evidence of time-delay-induced death in coupled limit-cycle oscillators,” *Phys. Rev. Lett.* **85**, 3381–3384 (2000).
- ²¹A. Stefanski, and T. Kapitaniak, “Steady state locking in coupled chaotic systems,” *Phys. Lett. A*, **210**, 279–282 (1996).
- ²²W. Zou, D. V. Senthilkumar, J. Duan, and J. Kurths, “Emergence of amplitude and oscillation death in identical coupled oscillators,” *Phys. Rev. E*. **90**, 032906 (2014).
- ²³T. Banerjee, and D. Biswas, “Amplitude death and synchronized states in nonlinear time-delay systems coupled through mean-field diffusion,” *Chaos* **23**, 043101 (2013).
- ²⁴A. Koseska, E. Volkov, and J. Kurths, “Oscillation quenching mechanisms: Amplitude vs. oscillation death,” *Phys. Rep.* **531**, 173–199 (2013).
- ²⁵A. Koseska, E. Volkov, and J. Kurths, “Transition from amplitude to oscillation death via Turing bifurcation,” *Phys. Rev. Lett.* **111**, 024103 (2013).
- ²⁶G. Gottwald, and I. Melbourne, “On the Implementation of the ϵ -Test for Chaos,” *SIAM J. Appl. Dyn. Syst.* **8**, 129–145 (2009).
- ²⁷J. Guckenheimer, and P. Holmes, *Nonlinear Oscillations, Dynamical Systems, and Bifurcations of Vector Fields*, (Springer, New York, 1986).
- ²⁸E. Ott, *Chaos in Dynamical Systems*, (Cambridge University Press, Cambridge, 2002).

- ²⁹H. D. I. Abarbanel, *Analysis of Observed Chaotic Data*, (Springer, New York, 1996).
- ³⁰H. Kantz, G. Radons, and H. Yang, “The problem of spurious Lyapunov exponents in time series analysis and its solution by covariant Lyapunov vectors,” *J. Phys. A-Math. Gen.*, **46**, 254009 (2013).
- ³¹S. Giannerini, and R. Rosa, “New resampling method to assess the accuracy of the maximal Lyapunov exponent estimation,” *Physica D* **155**, 101–111 (2001).
- ³²S. Giannerini, R. Rosa, and D. L. Gonzalez, “Testing chaotic dynamics in systems with two positive Lyapunov exponents: a bootstrap solution,” *Int. J. Bifurcat. Chaos* **17**, 169–182 (2007).
- ³³N. Marwan, M. Romano, M. Thiel, and J. Kurths, “Recurrence plots for the analysis of complex systems,” *Phys. Rep.*, **438**, 237–329 (2007).
- ³⁴E. J. Ngamga, A. Buscarino, M. Frasca, G. Sciuto, J. Kurths, and L. Fortuna, “Recurrence-based detection of the hyperchaos-chaos transition in an electronic circuit,” *Chaos*, **20**, 043115 (2010).
- ³⁵O. A. Rosso, H. A. Larrondo, M. T. Martin, A. Plastino, and M. A. Fuentes, “Distinguishing noise from chaos,” *Phys. Rev. Lett.* **99**, 154102 (2007).
- ³⁶F. Olivares, A. Plastino, and O. A. Rosso, “Contrasting chaos with noise via local versus global information quantifiers,” *Phys. Lett. A*, **376**, 1577–1583 (2012).
- ³⁷M. Sano, and Y. Sawada, “Measurement of the Lyapunov spectrum from a chaotic time series,” *Phys. Rev. Lett.* **55**, 1082–1085 (1985).
- ³⁸T. Kapitaniak, and L. O. Chua, “Hyperchaotic attractors of unidirectionally-coupled Chua’s circuits,” *Int. J. Bifurcat. Chaos* **4**, 477–482 (1994).
- ³⁹T. Kapitaniak, L. O. Chua, and G. Q. Zhong, “Experimental hyperchaos in coupled Chua’s circuits,” *IEEE T. Circuits-I* **41**, 499–503 (1994).
- ⁴⁰X. Wang, and M. Wang, “A hyperchaos generated from Lorenz system,” *Physica A*, **387**, 3751–3758 (2008).
- ⁴¹G. M. Mahmoud, M. A. Al-Kashif, and A. A. Farghaly, “Chaotic and hyperchaotic attractors of a complex nonlinear system,” *J. Phys. A-Math. Theor.*, **41**, 055104 (2008).
- ⁴²Y. R. Shen, *The Principles of Nonlinear Optics*, (John Wiley & Sons, Hoboken, 2003).
- ⁴³I. Sliwa, P. Szlachetka, and K. Grygiel, “Generation of strongly chaotic beats,” *Int. J. Bifurcat. Chaos* **18**, 835–840 (2008).
- ⁴⁴J. Cartwright, D. L. Gonzalez, and O. Piro, “Nonlinear dynamics of the perceived pitch of complex sounds,” *Phys. Rev. Lett.* **82**, 5389–5392 (1999).
- ⁴⁵E. Bradley, and H. Kantz, “Nonlinear time-series analysis revisited,” *Chaos* **25**, 097610 (2015).





1000

100

Hz

T12

Time

0.1

0.2

0.3

0.4

0.5

0.6

0.7

0.8

0.9

1.0

1.1

1.2

1.3

1.4

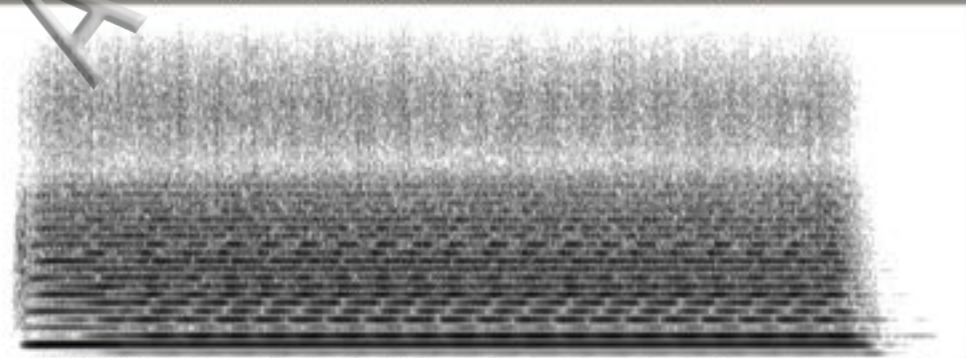
1.5

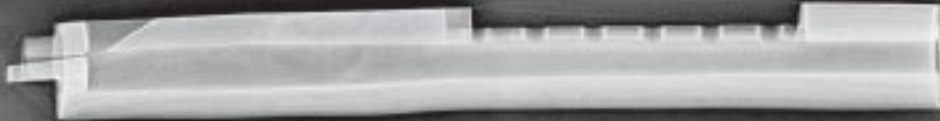
1.6

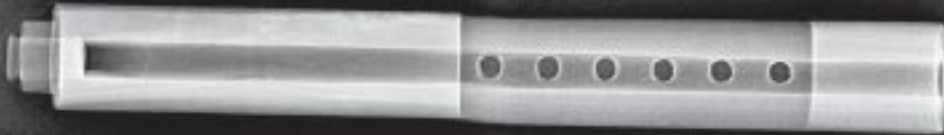
1.7

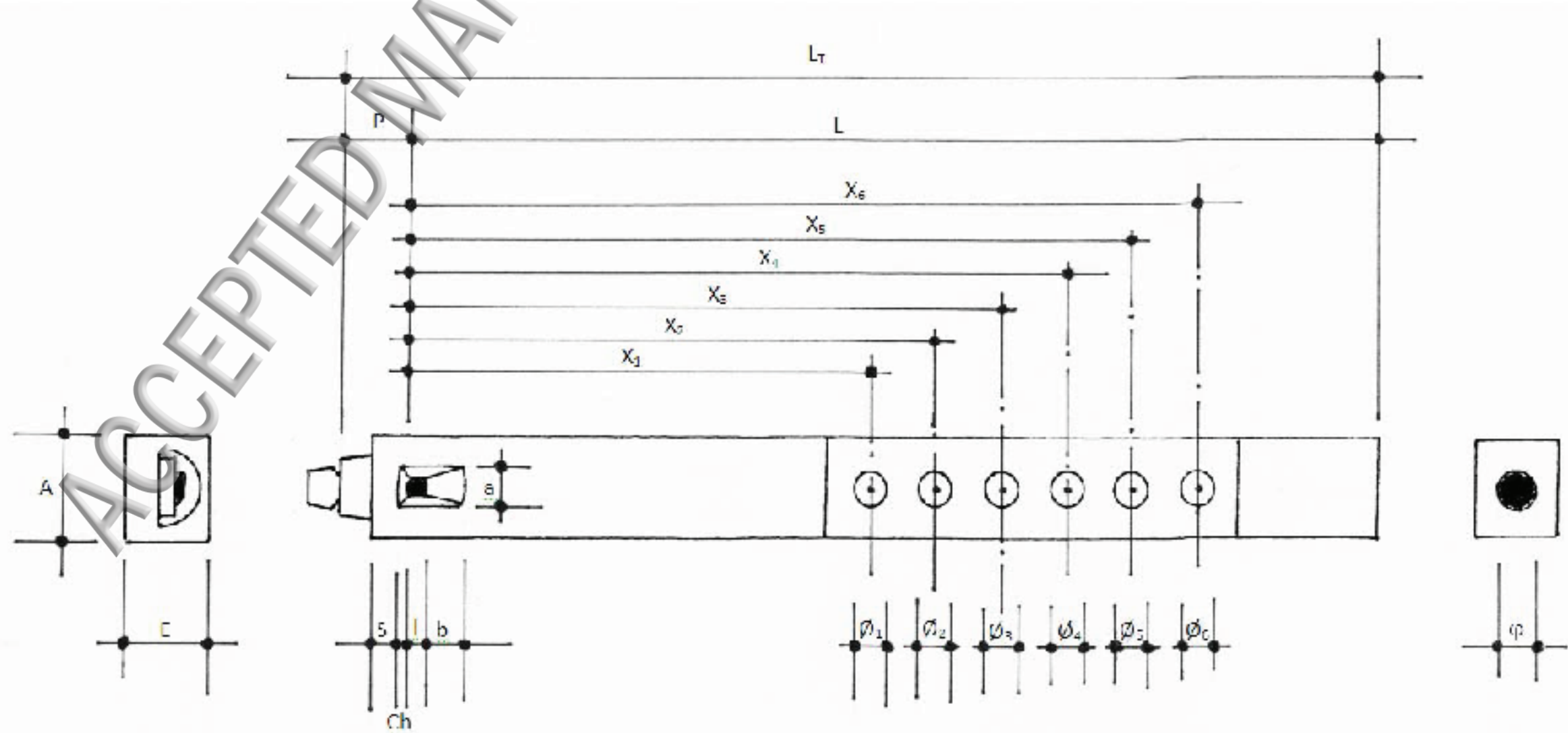
1.8

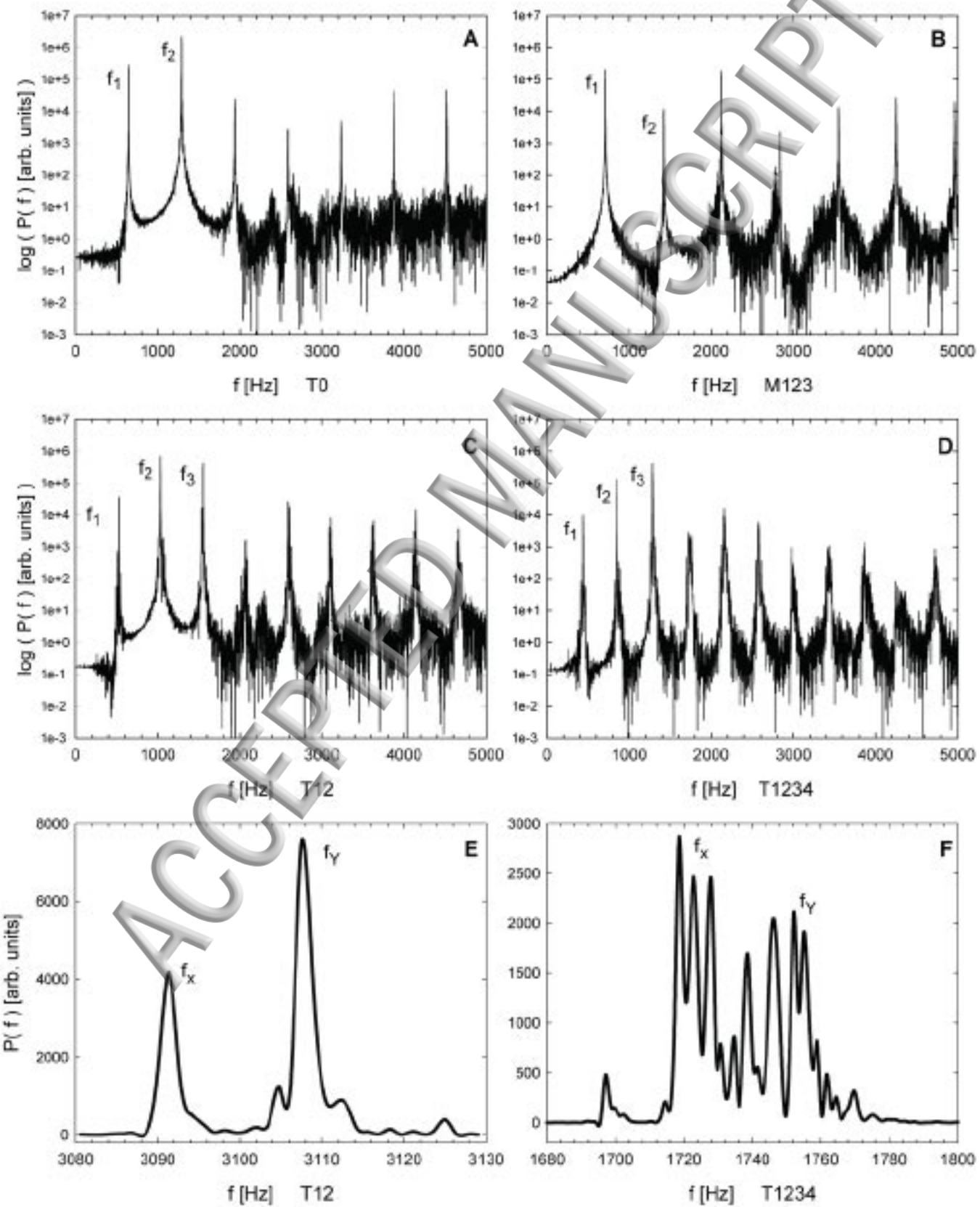
1.9

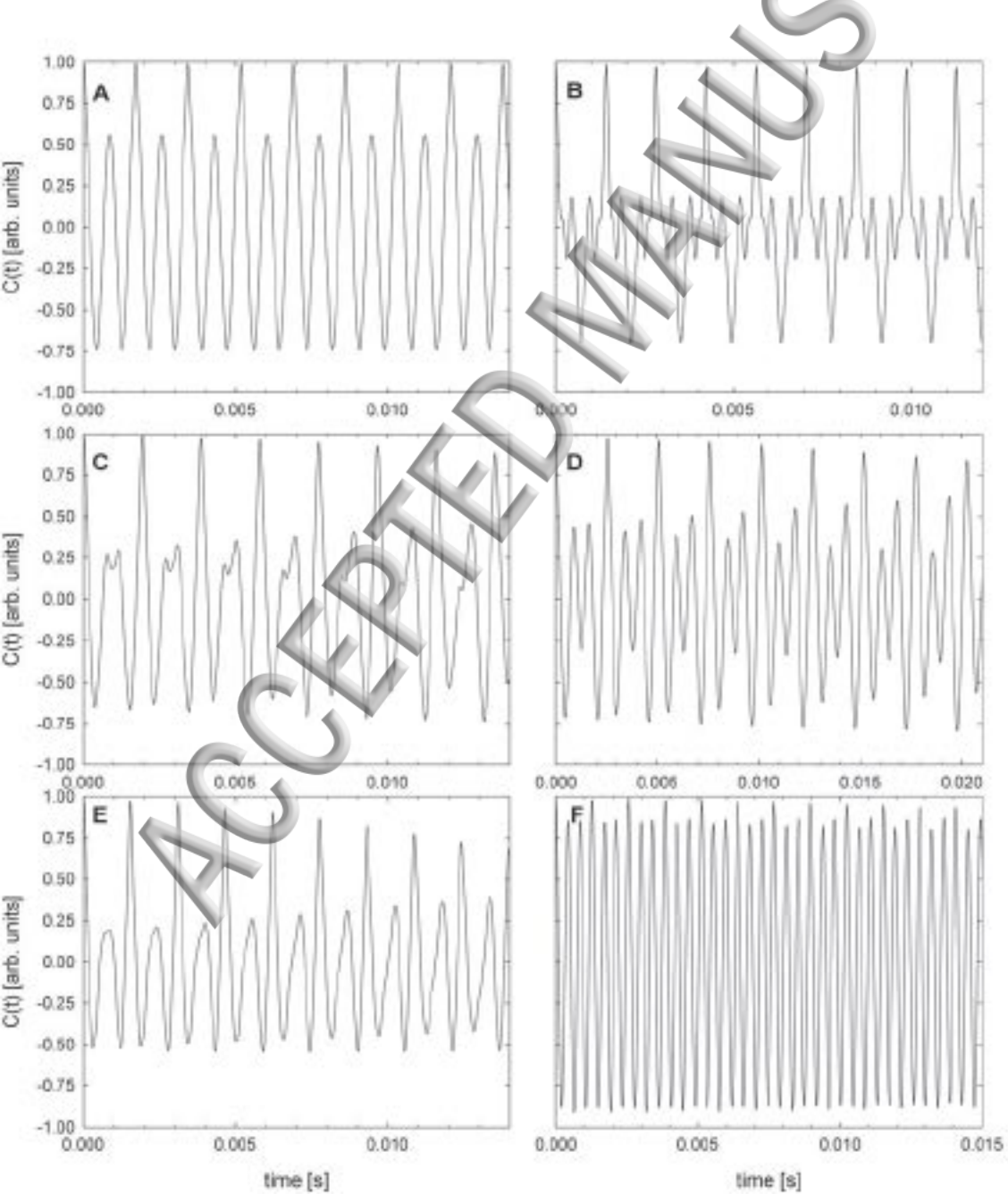




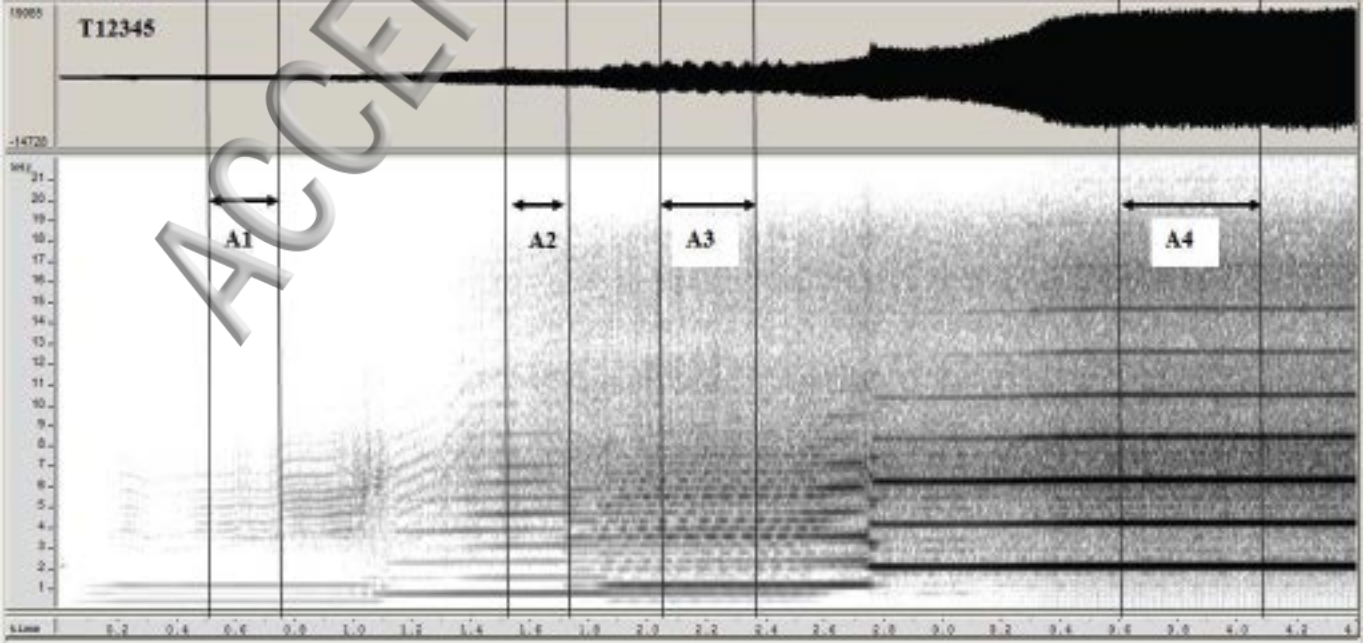








T12345



T1

1.9529

MHz

21
20
19
18
17
16
15
14
13
12
11
10
9
8
7
6
5
4
3
2
1

50MHz

0.7 0.8 0.9 1.0 1.1 1.2 1.3 1.4 1.5 1.6 1.7 1.8 1.9 2.0 2.1 2.2 2.3 2.4 2.5 2.6 2.7 2.8 2.9 3.0 3.1 3.2 3.3 3.4 3.5 3.7

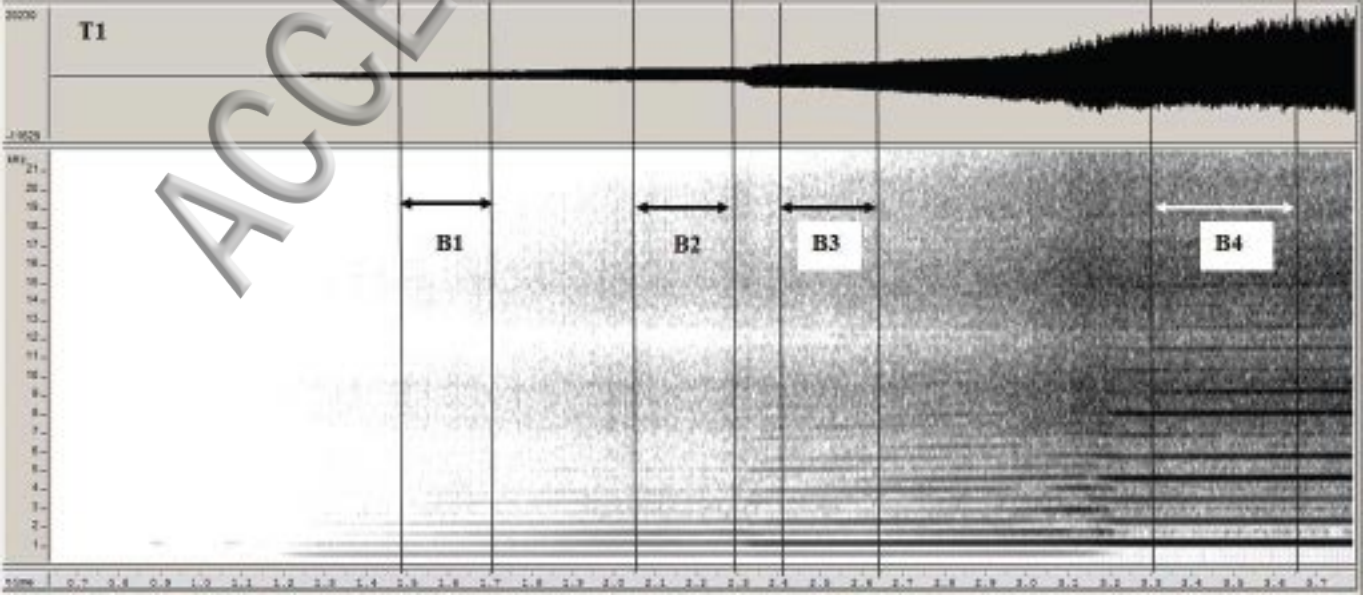
ACCEL

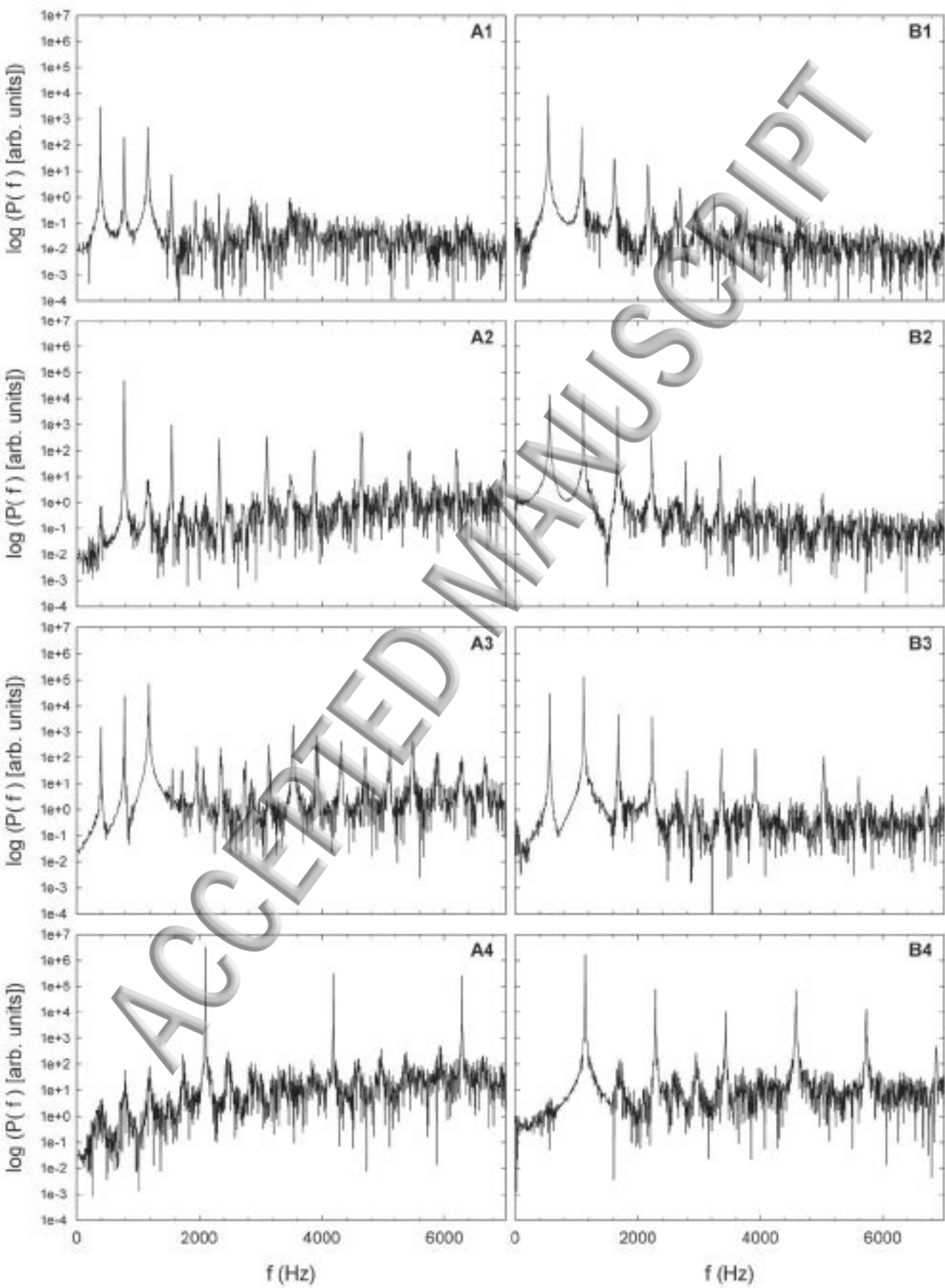
B1

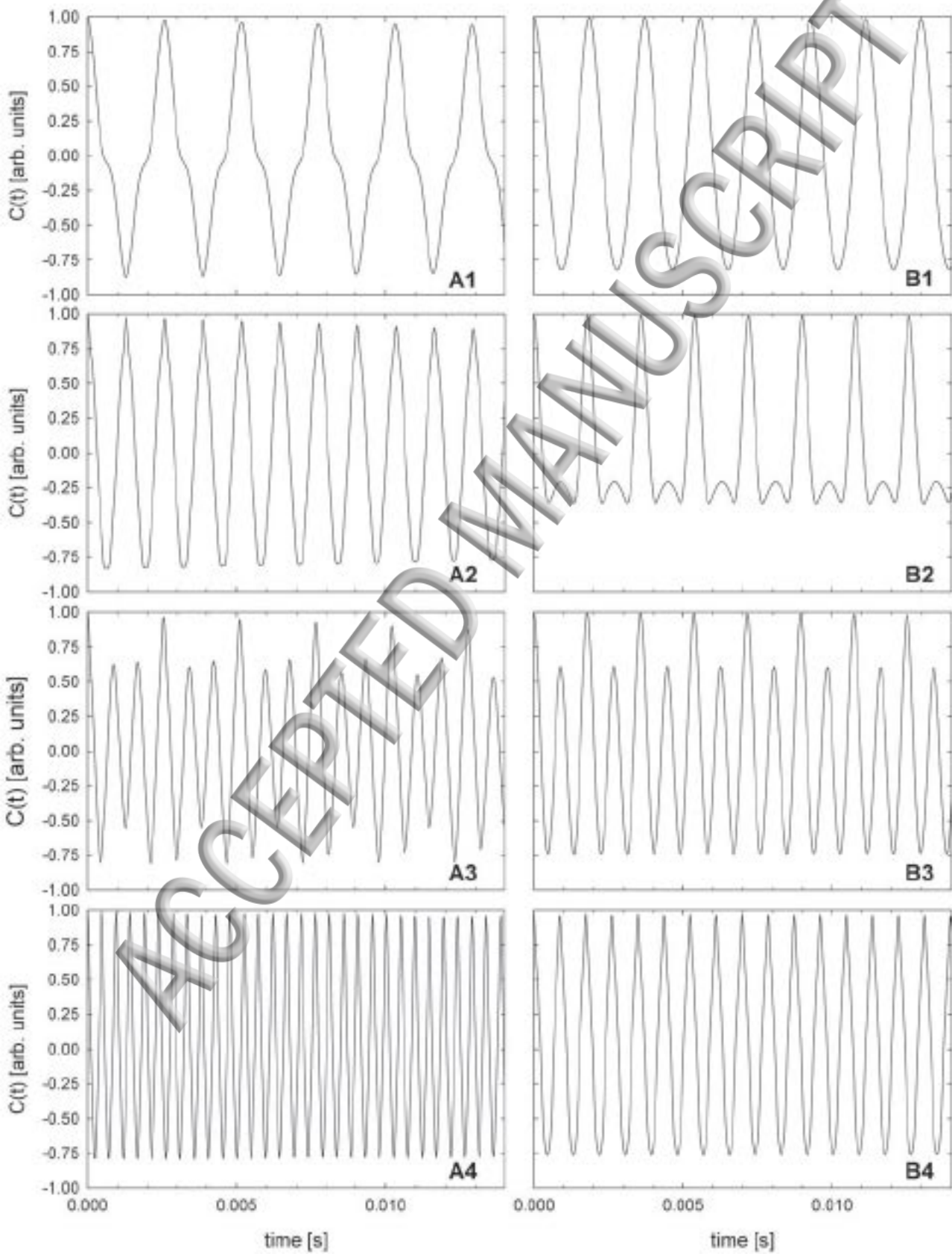
B2

B3

B4







Rel. Amp. [arb. units]

